Fizika Nizkikh Temperatur, 2009, v. 35, No. 4, p. 405–412

# Zero-phonon emission bands of solid hydrogen at 6–12 μm wavelength. An astrophysical phenomenon

J. Schaefer

*Max-Planck-Institut für Astrophysik, 1 Karl-Schwarzschild-Strasse, 85741 Garching, Germany*
E-mail: jas@mpa-garching.mpg.de

Received January 27, 2009

Infrared emission bands in the wavelength range of 6–12 μm observed in the ISO-SWS mission are assigned to rotational zero-phonon bands of solid parahydrogen by using Van Kranendonk's approximate rigid-lattice method. This method is based on superposed electric quadrupole pair interactions and superposed quadrupole induced dipole moments of pairs in the hcp crystal. Accordingly, the approximate formalism uses zero-order $H_2$ pair wave functions. Symmetry effects of the hcp crystal require preference of rotational pair transitions. The interaction potential of the pairs is confined to the electric quadrupole–quadrupole interaction. Zero-phonon emission bands of $H_2$ pair transitions fitted to the spectrum contain at least one delocalized $j = 2$ state initially and/or finally because of their significantly enhanced emission rates. They also yield the characteristic band widths which fit nicely to the widths of the observed features. The frequency positions of the seven pure parahydrogen pair transitions used, obtained from experimentally determined rotational solid hydrogen energy levels, are in perfect agreement with the observed features, whereas the three mixed ortho–para pair transitions need a presently unknown frequency correction, caused by the migration of the ortho-$H_2$ molecules into the parahydrogen crystal prior to emission, the so-called initial excess binding energies. The astrophysical setup of the observed source is discussed in the end of the paper.

PACS: 95.30.Gv Radiation mechanisms; polarization;
63.20.D– Phonon states and bands, normal modes, and phonon dispersion.

Keywords: emission band, zero-phonon emission, quadrupole–quadrupole interaction, ortho–para transition.

## 1. Introduction

Zero-phonon emission bands of solid hydrogen have not been measured yet in the laboratory, but an interesting information emerged which could initiate new activities in this particular field: the appearance of observed emission bands hypothetically related to dark baryonic matter in the Milky Way and in other spiral galaxies. Therefore, it seems to be an actual requirement to discuss a theoretical forecast of the simplest zero-phonon emission bands of solid hydrogen, meaning rotational transitions of $H_2$ molecules in the crystal which emit in the wavelength range of interest. This subject has been discussed already in a recently published paper of Schaefer (2007) [1].

There are three crucial aspects of the applied rigid-lattice approximation of Van Kranendonk [2] to be briefly introduced prior to the discussion of the characteristic features in the wavelength range between 6 and 12 μm.

At first, a rigorous pair approximation is assumed, based upon the validity of superposed pair interactions and superposed pair dipole moments of the $H_2$ molecules in the lattice and approximately confined to electric quadrupole interactions.

At second, the symmetry properties of the solid parahydrogen hcp crystal cause a characteristic cancellation effect valid in the rigid-lattice dipole moment function for single rotational transitions, whereas rotational pair transitions are not affected. The rotational $H_2$ pair transition is a dipole transition of two rotating $H_2$ molecules at nearest neighbor (nn) distance, where either one or both molecules undergo a rotational transition to emit or absorb one photon. Consequently, prominent dipole transitions are pair transitions, whereas single rotationally excited $H_2$ states in the ground-state crystal — with the exception of the $j = 2$ state — can be neglected in the discussion of prominent dipole radiation.

At third, since $H_2$, $H_2$ pairs and the parahydrogen crystal are Bose systems, the electric quadrupole–quadrupole interaction makes the $j = 2$ state energy «hopping» through the parahydrogen crystal; it is therefore called

«delocalized $j = 2$ state». If contributed to a pair transition initially and/or finally, it makes a great effect on the squared dipole transition matrix element, with an enhancement factor called «lattice sum». Therefore, pair transitions without a contributing delocalized $j = 2$ state are less important and may be expected to contribute to the background. Additionally, the typical band widths of the zero-phonon pair emission bands used are mainly caused by the energy spread of the delocalized $j = 2$ states in the lattice.

Details of Van Kranendonk's rigid-lattice approximation will be discussed in the following sections, i.e., the zero-order pair wave functions in Sec. 2, the dipole transitions of $H_2$ pairs in Sec. 3, widths and shifts of the emission bands in Sec. 4, and the effects caused by the depolarized $j = 2$ state in Sec. 5.

The actual zero-phonon emission spectroscopy is started in Sec. 6 by presenting the spectrum observed in the ISO-SWS mission and showing the discussed features between 6 and 12 μm wavelength, of a source located within the NGC7023 nebula, a so-called molecular cloud and photo-dissociation region (PDR) in the Milky Way. I should briefly mention the present state-of-the-art of the physical interpretation. The astrophysical community designates the source as mixture of polycyclic aromatic hydrocarbons (PAHs), more recently also as carbonaceous composites, and it could be probably assigned to many other molecules in the future. There is such a rich diversity of molecules available on Earth or accessible by chemical synthesis, that more molecules should be found by all means fitting somehow to the observed features. The theoretical and experimental work on the subject summarized under «PAHs» is quite impressive and highly professional, nevertheless, this paper is aimed at showing that the observed features are only emitted by visible hydrogen solids.

The prominent features in question have been fitted by using all available rotational pair transitions in this wavelength range with participating delocalized $j = 2$ states initially and/or finally. Seven of the ten prominent zero-phonon emission bands used are pure parahydrogen bands, the only ones available for testing the agreement with the observed features, with regard to frequency positions and estimated band widths. The frequency position is then determined by the difference of the experimentally determined initial and final energy levels. This simple procedure follows from the symmetry of the parahydrogen pairs. This symmetry does not apply to mixed ortho–para pairs because the substitutionally included ortho-$H_2$ impurities cause a distortion of the surrounding lattice molecules and a so-called «excess binding energy» of the initial $|JM\rangle$ pair states, with a frequency shift of the band. Hence the fits of these pair emission bands are rather artificial and not convincing.

Emission bands observed on both sides of the discussed wavelength range have not been included in the calculations, but their frequency positions help identify them as «extrapolations» of the prominent parahydrogen emission bands inside the wavelength range.

Minor important intensities inside and outside the discussed wavelength range could also be seen as pair transition bands, with a delocalized $j = 2$ state sharing a rotational single transition in the first excited vibrational level. This is more or less speculative and needs experimental proof.

Finally, in Sec. 7 the hypothetical astrophysical setup of the chosen observed source is briefly explained with the bright B-type star in the center of a sphere and observable as well as dark hydrogen solids outside. It explains infrared emission from the surroundings of young stars wherever they are located, at solar Galactic radius in the Milky Way or in spiral galaxies at remote regions of the Universe as observed in the SPITZER mission.

## 2. Zero-order pair wave functions

The consequence of the pair approximation are zero-order wave functions of $H_2$ pairs introduced to describe the physics in the rigid lattice. The formalism is known quite well from the physics of free pairs, where *ab initio* calculated interaction potentials and *ab initio* induced dipole moment functions have been used in collision induced radiation. I introduce zero-order pair wave functions

$$\psi^{JM}(\mathbf{R},\mathbf{r}_1,\mathbf{r}_2;j_1,j_2)=\sum_{jl}R^{-1}\bar{f}^{JM}_{j_1j_2jl}(R)I^{JM}_{j_1j_2jl}(\hat{\mathbf{r}}_1,\hat{\mathbf{r}}_2,\hat{\mathbf{R}}),$$

with an effective radial function which is normalized at the constant nn or rigid-lattice distance $R_0$ of the $H_2$ molecules at 3.75 Å:

$$\int dR\left|\sum_{jl}\bar{f}^{JM}_{j_1j_2jl}(R)\right|^2\delta(R-R_0)=1,$$

hence the pair wave function is also normalized. The angular part shows the coupling of $j_1$ and $j_2$,

$$I^{JM}_{j_1j_2jl}(\hat{\mathbf{r}}_1,\hat{\mathbf{r}}_2,\hat{\mathbf{R}})=\sum_{m_1m_2mm_l}C(j_1j_2j;m_1m_2m)\times$$

$$C(jlJ;mm_lM)Y_{j_1m_1}(\hat{\mathbf{r}}_1)Y_{j_2m_2}(\hat{\mathbf{r}}_2)Y_{lm_l}(\hat{\mathbf{R}}),$$

where the $C$′s are Clebsch–Gordan coefficients, and the $Y$′s are spherical harmonics. The angular momenta are coupled in the order of $j_1 + j_2 \to j$, and $j$ is coupled with the orbital angular momentum $l$ to the total $J$. The $m$′s are magnetic quantum numbers.

Now we must account for the fact the $H_2$, $H_2$ pairs and parahydrogen crystals are Bose systems. I shall note a dif-

ference: Mixed pairs of para- and ortho-$H_2$ contain distinguishable Bose particles, whereas pure parahydrogen pairs and pairs in the parahydrogen crystal are pairs of indistinguishable Bose particles. Their wave functions must be symmetrized with regard to the exchange of the molecules, and their interaction potential is symmetric in both directions.

Symmetrization of the pair wave functions is the basic condition of describing pairs in the parahydrogen crystal. Exchange of the molecules gives a new angular wave function

$$I^{JM(s)}_{j_1 j_2 jl} = [2(1+\delta_{j_1 j_2}\delta_{v_1 v_2})]^{-1/2} \times$$

$$\times [I^{JM}_{j_1 j_2 jl}(\hat{\mathbf{r}}_1, \hat{\mathbf{r}}_2, \hat{\mathbf{R}}) + (-1)^{j_1+j_2+j+l} I^{JM}_{j_1 j_2 jl}(\hat{\mathbf{r}}_1, \hat{\mathbf{r}}_2, \hat{\mathbf{R}})].$$

The two restricted symmetrized products, one for $j_1 \le j_2$ and the other one for $j_2 \le j_1$ are wave functions of parahydrogen free $(j_1, j_2)$ pairs as well as zero-order wave functions of the pairs in the parahydrogen solids.

The parity is obtained from $P_{12} = (-1)^{j_1+j_2+l}$ which shows, since $j_1$ and $j_2$ are even in parahydrogen, that obviously a change of the orbital angular momentum $l$ is required for the rotational dipole transitions of the pairs. This is a curiosity of the rigid-lattice pair approximation. We deal with that by assuming that any radiative dipole transition requires $l = 0$ initially, and the final orbiting energy is immediately transferred to the lattice, thus contributing to the phonon branches of the bands. It is a plausible assumption because an anisotropic coupling to the lattice vibrations exists. The final orbital angular momentum is consequently determined by the dipole moment function.

### 3. Dipole transitions of pair states

Dipole radiation is almost entirely made by the quadrupole induction mechanism, where the quadrupole $Q_2$ of molecule 1 polarizes molecule 2, the dipole moment is located on molecule 2, but it depends upon the orientation of molecule 1.

The rotationally invariant spherical expansion of the induced dipole moment function of an $H_2$ pair can be written in the form

$$\mu_v(\mathbf{R}_{ij}, \mathbf{r}_i, \mathbf{r}_j) = \frac{(4\pi)^{3/2}}{\sqrt{3}} \sum_{\lambda_1\lambda_2\Lambda L} B_{\lambda_1\lambda_2\Lambda L}(R_{ij}) \times$$

$$\times \sum_{m_1 m_2 M} C(\lambda_1\lambda_2\Lambda; m_1, m_2, m_1+m_2)\, C(\Lambda L 1; m_1+m_2, M, v) \times$$

$$\times Y_{\lambda_1 m_1}(\hat{r}_i) Y_{\lambda_2 m_2}(\hat{r}_j) Y_{LM}(\hat{R}_{ij}),$$

where the symbols $C$ and $Y$ are the same as already explained in Sec. 2.

Solid state symmetry effects are important:

– The $B_{022L}$ and the $B_{202L}$ terms are responsible for single rotational transitions and neglected in the parahydrogen solids because their induced dipole moments are proportional to the isotropic polarizability times the quadrupole moment, and the dipole moments on one side of the rotating molecule and the diametrically opposite one cancel, therefore, single $\Delta j = 2$ transition matrix elements are reduced by this so-called «cancellation effect». The cancellation is total in a perfect fcc crystal.

– By contrast, double rotational transitions of a pair at nn distance, determined by the $B_{22\Lambda L}$ terms with dipole moments $\propto \gamma$, the anisotropic polarizability, are not effected and are much stronger in the hcp crystal than single transitions (after Van Kranendonk). I conclude from that.

– Pair transitions dominate the rotational emission spectra of the $H_2$ molecules in solid hydrogen.

More specific details of solid hydrogen radiation can be found by looking at the approximate matrix element of dipole pair transitions obtained from the $B_{22\Lambda L}$ terms.

Integration over the angles gives

$$\langle J'M'l' | \mu_v | JM \rangle = \sum_{\Lambda L} B_{22\Lambda L}(R) 5 \sqrt{[\Lambda][L][j_1'][j_2'][J'][j_1][j_2][J]}\, (-1)^{j_1'+j_2'+l'+J'} \begin{pmatrix} j_1' & 2 & j_1 \\ 0 & 0 & 0 \end{pmatrix} \begin{pmatrix} j_2' & 2 & j_2 \\ 0 & 0 & 0 \end{pmatrix} \begin{pmatrix} l' & L & 0 \\ 0 & 0 & 0 \end{pmatrix} \times$$

$$\times (-1)^{\Lambda+L+J} \sum_{j'} \sqrt{[j']} \begin{pmatrix} \Lambda & L & 1 \\ J' & J & j' \end{pmatrix} \begin{pmatrix} j_1' & j_1 & 2 \\ j_2' & j_2 & 2 \\ j' & J & \Lambda \end{pmatrix} (-1)^{J'-M+v} \begin{pmatrix} J' & J & 1 \\ M' & -M & -v \end{pmatrix},$$

where $[j] \equiv 2j+1$, and the symbols in parentheses are 3-$j$, 6-$j$ and 9-$j$ Wigner symbols.

The Wigner symbols of this formula determine two additional interesting conditions of the matrix elements:

– the 3-$j$ symbol of the triple $\{l'L0\}$ in the second row requires odd $l'$ and odd $L = 1$ or 3, but only $L = 3$ (and $l' = 3$!) is significant, and that determines the final orbital angular momentum $l' = 3$;

– the triangle $\{\Lambda L 1\}$ in the third row yields three $\Lambda$'s: 2, 3 and 4, but only $B_{2233}$ is significant, with Tipping and Poll [3]:

$$B_{2233}(R) \to -\sqrt{\frac{2}{15}}(\gamma^{(1)}Q_2^{(2)} + Q_2^{(1)}\gamma^{(2)})R^{-4},$$

where the numbers in parentheses indicate the average over the intramolecular motion. Hence, there is only one term of the dipole moment expansion left in the rigid-lattice approximation.

### 4. Widths and shifts of the emission bands

The interaction potentials in the rigid lattice are also obtained from the interaction potential of pairs written in the rotational invariant form

$$V(\mathbf{R}_{ij}, \mathbf{r}_i, \mathbf{r}_j) = (4\pi)^{3/2} \sum_{l_1 l_2 K} V_{l_1 l_2 K}(R_{ij}, r_i, r_j) \times$$

$$\times \sum_{m_1 m_2 m} C(l_1 l_2 K; m_1 m_2 m) Y_{l_1 m_1}(\hat{\mathbf{r}}_i) Y_{l_2 m_2}(\hat{\mathbf{r}}_j) Y^*_{Km}(\hat{\mathbf{R}}_{ij}).$$

When considering only quadrupole interactions of the anisotropic parts and the symmetry effects found for the dipole moment transitions in the lattice, the only remaining anisotropy is the electric quadrupole–quadrupole term $V_{224}$, proportional to $R^{-5}$ asymptotically, and approximately at nn distance. It determines the specific widths of the rotational zero-phonon emission bands.

Normally several total $J$ and $J'$ states are defined by a rotationally excited $(j_1, j_2)$ pair, as, e.g., initially

$$|j_1 - j_2| \le J \le j_1 + j_2.$$

The potential matrix element of the $V_{224}$ term for a transition from $|JM\rangle$ states to $\langle \bar{J}\ \bar{M}|$ states integrated over the angles gives

$$\langle \bar{J}\ \bar{M} j_1 j_2 | V_{224} | JM j_1 j_2 \rangle = 15\delta_{M\bar{M}} V_{224}(R)[j_1][j_2]\sqrt{[\bar{J}][J]} \times$$

$$\times \begin{pmatrix} j_1 & 2 & j_1 \\ 0 & 0 & 0 \end{pmatrix} \begin{pmatrix} j_2 & 2 & j_2 \\ 0 & 0 & 0 \end{pmatrix} \begin{pmatrix} j_1 & j_1 & 2 \\ j_2 & j_2 & 2 \\ \bar{J} & J & 4 \end{pmatrix} \times$$

$$\times (-1)^{j_1 + j_2 + J - M} C(\bar{J} J 4; \bar{M} - M 0),$$

with the results that $\bar{M} = M$ is required, whereas $J$ is not conserved by the EQQ term, therefore, the initial zero-order $|JM\rangle$ pair states with $l = 0$ split into components of $|M\rangle$ states which has been included in the calculated band widths of the zero-phonon emission bands. A similar splitting has been calculated for the final $\langle J'M'|$ states obtained from

$$|j_1' - j_2'| \le j' \le j_1' + j_2', \quad |j' - 3| \le J' \le j' + 3.$$

The splitting result in an effective frequency shift of the bands which is shown below. I skip the details. I may note, all these splittings are local, bound to the local pair at nn distance.

### 5. Effects caused by the delocalized $j = 2$ state

The largest contribution to the band widths, by far more significant than all local $|JM\rangle$ and $\langle J'M'l' = 3|$ splittings, is made by the energy spread of the $j = 2$ state over the parahydrogen crystal, therefore called «delocalized $j = 2$ state», an effect of the quadrupole–quadrupole interaction term applied to the symmetric pair wave function of a single $j = 2$ state in the ground-state crystal yielding

$$\left\langle \psi_{02}^{2,\bar{m}} \middle| EQQ \middle| \psi_{02}^{2m} \right\rangle =$$

$$= EQQ(R) \int d\hat{\mathbf{r}}_1 d\hat{\mathbf{r}}_2 d\hat{\mathbf{R}}; I_{02}^{2\bar{m}} EQQ(\hat{\mathbf{R}}, \hat{\mathbf{r}}_1, \hat{\mathbf{r}}_2) I_{20}^{2m}.$$

The result is an exchange of $j = 2$ in the angular part of the matrix element from $I_{20}$ to $I_{02}$. This matrix element is called «hopping matrix element» because the energy of the $j = 2$ state is transferred to the other pair molecule, similar to the next one and so on, to the parahydrogen molecules in the crystal.

The potential terms responsible for single rotational transitions do not contribute to the «hopping». This is another reason for neglecting them.

Evaluation of the matrix element for the transitions of the $j = 2$ state energy between the positions $\mathbf{R}_i$ and $\mathbf{R}_j$ gives the general expression

$$\langle 2m, \mathbf{R}_i | EQQ | 2n, \mathbf{R}_j \rangle = \sqrt{70}\, \frac{Q_2 Q_2}{5R_{ij}^5} (-1)^m \times$$

$$\times C(224; m - n(m-n)) \frac{\sqrt{4\pi}}{3} Y_{4(n-m)}(\hat{\mathbf{R}}_{ij}),$$

where a transition of the $z$ components from $n$ to $m$ is included because of different orientations of the $H_2$ molecules in the lattice.

Solid state theory tells us: The hopping motion of the $j = 2$ state through the lattice is described by the Bloch wave, with the amplitude determined by the hopping matrix elements. But this formalism has not been applied yet to the parahydrogen crystal. Calculated estimates of the line widths (provided by Van Kranendonk) and an available data of an absorption band measured by Balasubramanian et al. (1982) [4] can be used for a roughly estimated general typical emission bandwidth.

It will be generally assumed that each initial and/or final $j = 2$ state at the vibrational $H_2$ ground-state level, occurring in a rotational pair transition $J'M' \leftarrow JM$ in the parahydrogen lattice, contributes with $\approx 20$ cm$^{-1}$ to the width of this band.

There is a second important effect of the delocalized $j=2$ state in dipole moment pair transitions, a significant enhancement factor of the squared dipole moment matrix elements, called «lattice sum *S*». It applies to all transitions of pair states with a delocalized $j=2$ state initially and/or finally.

Van Kranendonk used the summation method of Nijboer and Wette [5] and calculated a lattice sum of 12.8 enhancing the (local) squared dipole moment matrix elements of the $S(0)+S(0)$ absorption coefficient by including the induction of the delocalized $j=2$ states in about two to three hundred neighbors of the local pair. Proof has been provided in a measurement by Kiss [6]. I will not repeat this procedure, but use Van Kranendonk's results for a general estimated enhancement factor: $S$ = 6.4 will be applied to the rotational squared dipole moment matrix element $\left|\langle J'M'j_1'j_2'|\mu_\nu|JMj_1j_2\rangle\right|^2$ for each $j=2$ state involved initially and/or finally.

Consequently, rotational pair transitions not including a $j=2$ state molecule are smaller by this factor and are expected to occur normally in the background. Now I have all the tools for an approximate calculation of solid hydrogen zero-phonon emission bands.

The computational procedure of calculating band emission profiles starts with the calculation of the local EQQ splitting and shifts. Then the squared dipole moment matrix elements of the $JM \to J'M'$ transitions are calculated, $\left|\langle J'M'j_1'j_2'|\mu_\nu|JMj_1j_2\rangle\right|^2$ with initial $l=0$ and final $l'=3$, as required by the $B_{2233}$ term. The correct zero-phonon approximation would then continue with the calculation of the effective band width and the effective «lattice sum *S*» of each *JM* transition caused by the delocalized $j$ = 2 state. Programs for this are not available, therefore, the provisional estimates of 20 (40) wavenumbers for the effective width and an enhancement factor of 6.4 (12.8) are used to obtain the contribution of each squared matrix element to the band profile of the pair transition with an assumed Gaussian profile placed at the experimental band transition frequency and corrected by the resulting local EQQ shift.

With an intermediate expression for the sum over the magnetic quantum numbers, over the polarizations, and over the final total angular momentum [7],

$$\left|\langle j_1'j_2'|\boldsymbol{\mu}|j_1j_2J\rangle\right|^2 =$$

$$= \frac{1}{(2J+1)}\sum_{J'}\sum_{M'M\nu}\left|\langle J'M'j_1'j_2'|\mu_\nu|JMj_1j_2\rangle\right|^2,$$

the emission rate of the zero-phonon band is obtained in the form

$$A(j_1'j_2' \leftarrow j_1j_2) = \frac{32\pi^3}{3}\frac{\Delta E^3}{h^3c^3}\frac{e^2}{\hbar}\times$$

$$\times\frac{a_0^2}{(2j_1+1)(2j_2+1)}\sum_J\left|\langle j_1'j_2'|\boldsymbol{\mu}|j_1j_2J\rangle\right|^2.$$

The theory is now applied to the infrared emission spectrum observed in the ISO-SWS mission.

### 6. Spectroscopy of rotational pair transitions

The source has been the prominent photo-dissociation region (PDR) of the NGC7023 (Iris) nebula. I will describe the astrophysical conditions of this radiation at the end of my paper. The observed spectrum is shown in Fig. 1.

First to be mentioned are the nicely resolved gas phase quadrupole transition lines of $H_2$ marked on top of the figure, ranging from $S(1)$ up to $S(5)$, emitted in locally separated gas regions of this prominent PDR, where a mixture of H and excited $H_2$ gas can be observed. We know they are emitted from low-density gas sources because collisional relaxation of excited $H_2$ gas interacting with $H_2$ or H prevails already at reasonable gas densities much smaller then those above the solids.

There are four features marked with roman numbers to be explained by using ten bands of rotational pair transitions of solid $H_2$. I may note again: these are rotational pair transitions which include at least one delocalized $j=2$ state initially or finally.

Three different types of pair transitions have been used:

– both molecules relax in 6 bands,

– the $j=2$ state is excited in 3 bands,

– and one band is a single transition $S(4)$ with a $j=2$ partner at nn distance.

The transition wavenumbers are shown in Table 1.

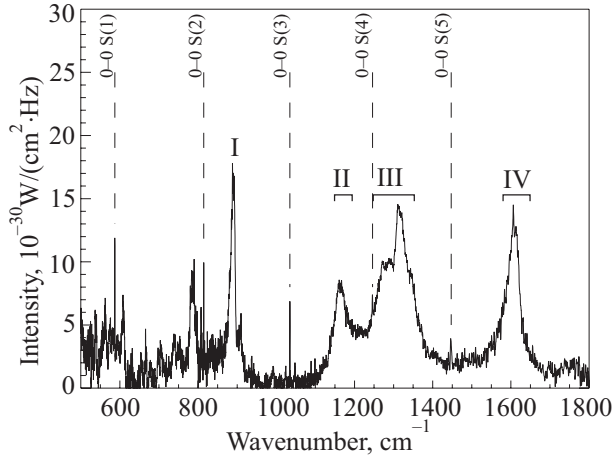


*Fig. 1.* The emission spectrum of the NGC7023 (Iris) nebula.

Table 1. Wavenumbers of transition

| No. | Transition | $\Delta E$, cm$^{-1}$ |
|---|---|---|
| I | $S(1) + S(0)$ | 941.47 – x |
| | $S(4) - S(0)$ | 887.84 (exp) |
| II | $S(2) + S(0)$ | 1167.1 (exp) |
| | $S(4)$ with a $j = 2$ host | 887.84 (exp) |
| II | $S(6) - S(0)$ | 1278.18 (exp) |
| | $S(3) + S(0)$ | 1389.14 – x |
| | $S(1) + S(2)$ | 1396.9 – x |
| IV | $S(4) + S(0)$ | 1599. (exp) |
| | $S(2) + S(2)$ | 1623.0 (exp) |
| | $S(8) - S(0)$ | 1625. |

Experimentally determined energy levels of $H_2$ in solid hydrogen up to $j = 8$ can be used to determine the frequency positions of the pure parahydrogen emission bands, i.e., the pair transition frequencies are simply determined by the sum of the experimental $S(j)$ ($\Delta j = 2$) energies marked with «exp». The energy levels of the ortho-$H_2$ species observed in absorption as single impurities or mixed ortho–para pairs cannot be used this way. The ortho-$H_2$ impurity normally migrates slowly into the parahydrogen solid, where «slowly» means: the ortho–para pair emission rates in solid hydrogen may be generally expected small enough to normally assume a completed migration process prior to emission. I shall note that the migration process of the final state starts up after radiation, therefore, only the excess binding energies of the initial pair states produce a shift of the transition frequency. In more detail, the $2j+1$ possible orientations of an ortho-$H_2$ $j$ state in the lattice give rise to generally $2j+1$ different local distortions with $R_{ij}$ distances $\neq R_0$, as determined by the orientation-dependent interaction. Consequently, all the $2j+1$ excess binding energies must be evaluated and averaged.

Significant band widths as well as large excess binding energies can be expected for mixed ortho–para pairs containing initially an excited ortho-$H_2$ $j$ state and a delocalized $j = 2$ state, where contributions to the effective band widths as well as to the averaged excess binding energies exceed by far the range of the next shell around the ortho-$H_2$ impurity. Efforts of doing this computationally have not yet been started.

The calculated emission profiles are finally expressed in Jansky units ($10^{-30}$ W/cm$^2$·Hz) for the comparison with the measurement and multiplied with an appropriate scaling factor fitted to the observed band intensity, keeping in mind that some phonon radiation should be included in the fits, normally expected on the blue side of the bands. The Fig. 2 contains the result of this procedure.

I will discuss, first of all, the 7 pure parahydrogen bands by comparing their frequency positions with the positions of the observed features and by comparing their estimated band widths with the required band widths of the observed features. I want to note: all observed band widths have been the same at all observed sources!

– The first parahydrogen band in feature I, $S(4)$–$S(0)$ at 888 wavenumbers, shares the intensity with the mixed ortho–para $S(1) + S(0)$ band. This is an assumption based on the expected large excess binding energy of the $S(1) + S(0)$ band. The width of the $S(4)$–$S(0)$ band of $\approx 20$ wavenumbers is reasonable, but the portions of flux distributed by the two bands are uncertain.

– Feature II is in perfect agreement with the double de-excitation band $S(0) + S(2)$ at 1167 wavenumbers, considering the position and band widths, and an expected phonon intensity on the blue side.

– The next parahydrogen pair transition band $S(6)$–$S(0)$ at 1278 wavenumbers does not show up with a separate feature, however, it explains the measured flux at the right position. (The fit neglects a small shift to the red side and some minor extra splitting due to spin–lattice coupling called «self-energy shift» of the $j = 8$ state.) There is no pair transition known explaining the intensity on its red side,

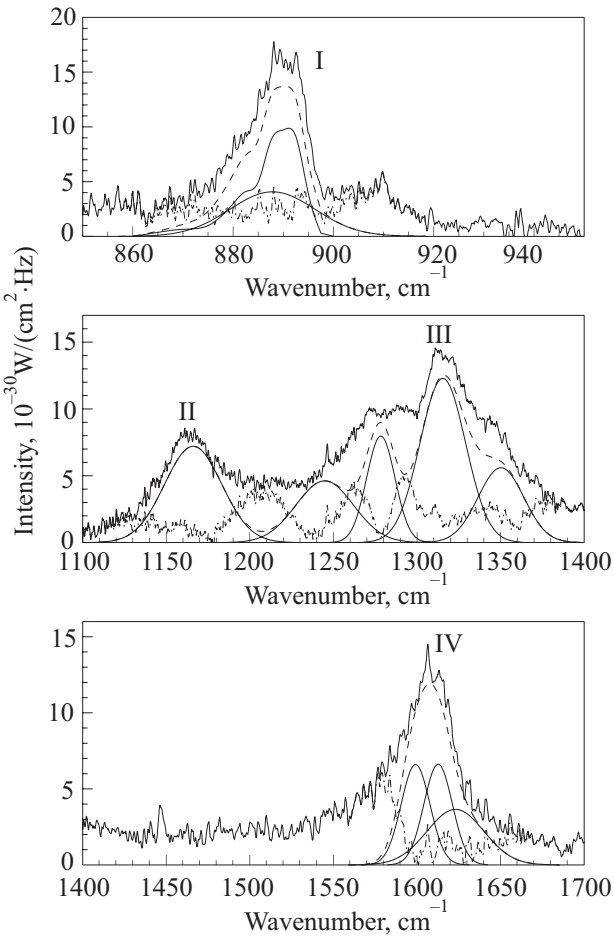


*Fig. 2*. The same as in Fig. 1. but with the calculated emission profile.

but a single $S(4)$ transition at 1243 wavenumbers with an unchanged $j = 2$ partner at nn distance fits in at the right position with reasonable band width.

– The next two bands are mixed ortho–para bands available to fit the rest of the feature lebeled III.

– The feature IV is fitted with three emission bands, starting with the $S(4) + S(0)$ band on the red side at 1599 wavenumbers. Additional intensity on the red side could be explained again by a single rotational transition $S(6)$ in the first vibrational level, at ≈1553 wavenumbers with a $j = 2$ partner and a width of 40 wavenumbers. It is not included in the fit. The $S(8)$–$S(0)$ band at ≈1612 wavenumbers with ≈ 20 wavenumbers width and the $S(2) + S(2)$ band at 1623 wavenumbers with ≈ 40 wavenumbers width fit properly to the frequency position and to the width of the feature IV.

Despite of expected changes of the calculated band profiles to be provided in the future, I am able to state perfect agreement of the zero-phonon band positions and useful band widths of the seven pure parahydrogen bands presented as convincing facts in favor of assignable interstellar solid hydrogen sources.

In contrast to this result, the transition frequencies of the three bands of mixed ortho–para pairs cannot be shown in agreement with measurements because of their unknown initial excess binding energies and their unknown profiles, certainly not Gaussian. And even their portions of intensity contributing to the measured features are unclear, therefore, their fits shown in the figure are largely artificial. More work is needed to do better.

The fitted flux and the calculated emission rates of the zero-phonon bands are used to determine pair column densities of the source. The SWS aperture has been $14\times20$ arcsec$^2 \equiv 6.5812\cdot10^{-9}$ rad. Assuming a source distance of ≈ 440 pc ($1.3574\cdot10^{19}$ m), it spans an area of $1.2\cdot10^{30}$ m$^2$. The flux density corrected for the aperture and the emission rate $A_{\rm if}$ [sec$^{-1}$] determine the (averaged) column density of the observed pair transition, $N = 4\pi\lambda$ Flux/($hcA_{\rm if}$) [cm$^{-2}$]. Filling factors of the sources are unknown. Estimates of column densities are shown in Table 2, last column. They are as much uncertain as the estimated emission rate coefficients.

It needs a cloud of several parsec depth and a huge amount of hydrogen solids to explain these column densities summed over many different sources.

Also shown are the three significant still uncertain excess binding energies of the mixed ortho–para bands and the small calculated effective shifts of the pure parahydrogen bands caused by the local splitting at fifth column and estimated emission rates at sixth column.

Less significant single transitions with participating $j = 2$ states at 6–12 μm wavelengths have not been calculated but should be mentioned: The shoulder above 1600 wavenumbers could contain a small contribution of the $S(6)$ band with a width of ≈ 40 wavenumbers. And some $S(j)$ transitions in the first vibrational excited level could also contribute to shoulders, as, e.g.

$1-1S(4)$ at ≈1180 cm$^{-1}$,

$1-1S(5)$ at ≈1370 cm$^{-1}$,

$1-1S(6)$ at ≈1553 cm$^{-1}$.

Of course, solid hydrogen emission bands can also be found outside the 6–12 μm wavelength interval, again with participating $j = 2$ states and ≈ 40 cm$^{-1}$ widths:

below 800 cm$^{-1}$: the $0-0S(2)$ and the $1-1S(2)$ band,

below 610 cm$^{-1}$: the $0-0S(1)$ and the $1-1S(1)$ band.

The series of de-excitation plus excitation pairs has been started with the $S(4)$–$S(0)$ band. It should be continued to include also the $S(2)$–$S(0)$ pair transition at ≈ 22 μm (450 cm$^{-1}$). And indeed, it has been observed twice in the ISO mission at the Carina nebula, together with a single $S(0)$ band at ≈ 28 μm (356 cm$^{-1}$), both with at least 40 cm$^{-1}$ widths. The complete width of this double band is not yet clear because of different beams used below and above 27.5 μm, therefore, I did not apply calculations.

Table 2. The parameters of the features I–IV of Fig. 2.

| No. | Band in $v = 0$ | $\Delta E$, cm$^{-1}$ | Width, cm$^{-1}$ | Shift, cm$^{-1}$ | $A_{\rm if}$, $10^{-6}$sec$^{-1}$ | Flux, $10^{-18}$ W/cm$^2$ | $N$, $10^{16}$ cm$^{-2}$ |
|---|---|---|---|---|---|---|---|
| I | $S(1) + S(0)$ | 941.47 (exp) | | ≈ –54.6 | 4.62 | 3.69 | 8.63 |
| | $S(4) - S(0)$ | 887.84 (exp) | 20.0 | – 0.06 | 2.47 | 2.59 | 11.4 |
| II | $S(2) + S(0)$ | 1167.1 (exp) | 40.0 | – 1.05 | 39.4 | 9.25 | 1.94 |
| III | $S(4)$ | 1243.44 (exp) | 40.0 | + 1.31 | 7.92 | 5.98 | 5.84 |
| | $S(6) - S(0)$ | 1278.18 (exp) | 20.0 | + 0.08 | 7.36 | 5.08 | 5.19 |
| | $S(3) + S(0)$ | 1389.14 (exp) | 32.0 | ≈– 73.8 | 13.0 | 12.6 | 7.06 |
| | $S(1) + S(2)$ | 1396.9 (exp) | 32.0 | ≈ –46.8 | 21.3 | 5.73 | 1.91 |
| IV | $S(4) + S(0)$ | 1599.04 exp | 20.0 | – 0.01 | 42.9 | 4.26 | 0.597 |
| | $S(8) - S(0)$ | 1612.5 | 20.0 | | 14.5 | 4.22 | 1.74 |
| | $S(2) + S(2)$ | 1623.00 (exp) | 40.0 | – 0.09 | 50.2 | 4.67 | 0.551 |

The general series of rotational double de-excitation emission bands is expected to continue above 1600 wavenumbers, up to about 3000 wavenumbers, where the emission bands of nrs IX and X overlap, containing transitions from up to $j = 13$ and 12, respectively. Above 3000 wavenumbers starts a new pair transition series, the $1\text{-}0O(j) + S(0)$ series. In front of those we have a generally observed feature at $\approx 3040$ wavenumbers probably built up from some $1\text{-}0O(j) - S(0)$ pair transitions. Expecting still a dominant role of the delocalized $j = 2$ state in pair transitions at this frequency range seems to be an appropriate assumption.

### 7. The astrophysical phenomenon

Hydrogen solids should be formed already in the halos of a spiral galactic, which is not discussed here. It means baryonic dark matter is available to form stars either at the edges of the optical galactic disks or in socalled molecular clouds.

The distance between a star and the position of the source is important for observing solid hydrogen, because in surroundings close to the star solid hydrogen either evaporates completely shortly after the star starts burning, or heavy planets gained sufficient gravitational attraction to retain their hydrogen at surfaces. The situation is different at larger distances, where the selfshielding atmospheres of hydrogen solids are opaque for the dissociative radiation from the star, and the supersonic hydrogen atoms produce a shock front in front of the solids.

This situation has been found in the ISO mission at the prominent PDR of the NGC7023 (Iris) nebula, where we have a scheme published by Fuente et al. [8], see Fig. 3, showing H column density maps in contours, $^{13}CO$ abundances in grey scales observed by Fuente et al. [9], and filaments in $H_2$ fluorescent emission observed by Lemaire et al. [10]. The SWS beam of 14×20 arcsecs squared has been included in the figure. $H_2$ fluorescent emission has been observed there and shown in the SWS spectra, I refer to the gas phase emission lines in Fig. 1. The circle shows the beam of the ISO long wavelength spectrometer.

Solid hydrogen is expected to be observable behind the fluorescent emission at about 60 arcsecs distance from the star. Assuming a source distance of ≈ 440 pc (parsec), the distance from the star is about 0.128 pc (≈ 26000 A.U.; Pluto's maximum distance from the Sun is 49 A.U.) and the SWS source observed in the middle of the rectangular beam is located approximately 0.114 pc outside the projection plane which contains the star, on one or on both sides of the sphere with radius 0.128 pc around the star.

I assume that part of the supersonic H penetrates the shock front and recombines in the solids at temperatures

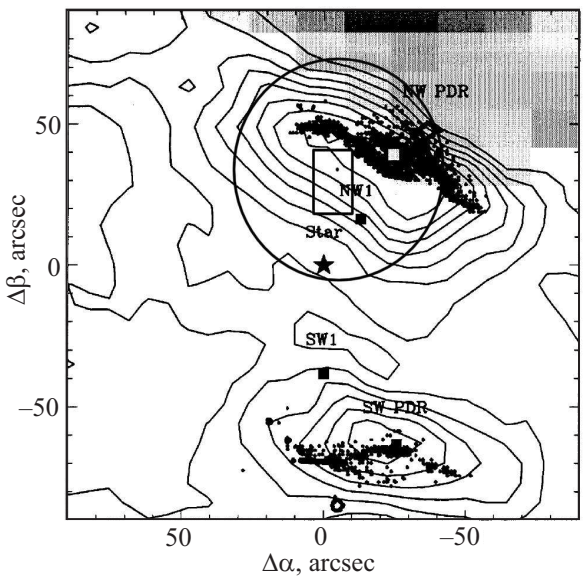


*Fig. 3.* The emission spectrum of the NGC7023 (Iris) nebula.

below the triple point of 13.8 K. It is plausible to further assume a great part of the $H_2$ binding energy being collisionally transferred to surrounding lattice molecules prior to restoration of the crystal structure. The result is a much smaller ratio of excited ortho/para $H_2$ abundances after recombination than the statistical ratio of 3:1. The last steps of radiative relaxation are expected to be rotational pair transitions at zero vibrational level to be observed in the frequency range of the ISO-SWS, where solid hydrogen as a relatively weak source, meaning a huge amount of hydrogen solids of unknown sizes, became observable in the interstellar space.

1. J. Schaefer, *Chem. Phys*. **332**, 211 (2007).
2. J. Van Kranendonk, *Solid Hydrogen*, Plenum Press, N.Y. (1983).
3. R.H. Tipping and J.D. Poll, in: *Molecular Spectroscopy: Modern Research*, Vol. III, K. Narahari Rao and C. Weldon Mathews (eds.), Academic Press Inc., London (1985), p. 421.
4. T.K. Balasubramanian, C.H. Lien, J.R. Gaines, K. Narahari, and E.K. Damon, *J. Mol. Spectr*. **92**, 77 (1982).
5. B.R.A. Nijboer and F.W. De Wette, *Physica* **23**, 309 (1957).
6. Z.J. Kiss, *Ph.D. Thesis*, University of Toronto, Toronto, Ontario (1959).
7. E.U. Condon and G.H. Shortley, *The Theory of Atomic Spectra*, Cambridge University Press (1967).
8. A. Fuente, J. Martin-Pintado, N.J. Rodriguez-Fernández, J. Cernicharo, and M. Gerin, *A&A* **354**, 1053 (2000).
9. A. Fuente, J. Martin-Pintado, N.J. Rodriguez-Franco, and G.D. Moriarty-Schieven, *A&A* **339**, 575 (1998).
10. J.L. Lemaire, D. Field, M. Gerin, S. Leach, G. Pineau des Forêts, F. Rostas, and D. Rouan, *A&A* **308**, 895 (1996).